JOM, Vol. 70, No. 11, 2018
https://doi.org/10.1007/s11837-018-3134-3




# Precipitation Behavior of IN718 After Surface Mechanical Attrition Treatment (SMAT) and Its Effect on Wear Properties

ANUJ BISHT,[1,2,4] SUPREETH GADDAM,[3,5] LAILESH KUMAR,[2,6] B.P. DILEEP,[3,7] and SATYAM SUWAS[2,8]

1.—Centre for Nanoscience and Engineering, Indian Institute of Science, Bangalore 560012, India. 2.—Department of Materials Engineering, Indian Institute of Science, Bangalore 560012, India. 3.—Department of Mechanical Engineering, Amrita School of Engineering, Amrita Vishwa Vidyapeetham, Bangalore 560035, India. 4.—e-mail: toninegi01@gmail.com. 5.—e-mail: supreeth.gaddam@gmail.com. 6.—e-mail: kumarlailesh.mit@gmail.com. 7.—e-mail: bp_dileep@blr.amrita.edu. 8.—e-mail: satyamsuwas@iisc.ac.in

Inconel 718 is a precipitation-strengthened Ni-based superalloy which finds applications across a wide temperature range (up to 650°C). It shows excellent yield strength, ductility, creep resistance and fatigue strength. Surface treatment is known to improve the fatigue life of materials via nano-crystallization of the surface layer. However, the precipitation behavior of the surface-treated layer is largely unexplored. In this regard, the present study aims to investigate and compare the precipitation in the surface-treated layer and the bulk solution-treated IN718. The material is subjected to surface mechanical attrition treatment (SMAT) after solution treatment and is followed by a two-step aging treatment which promotes the precipitation of $\gamma''/\gamma'$ in the alloy. The precipitation behavior shown by the bulk and SMAT layer was different. After aging, the bulk shows a microcrystalline $\gamma$ matrix containing $\gamma''$ precipitates, whereas the microstructure of the surface layer consists of nanograins with nanotwins. No evidence of $\gamma''/\gamma'$ precipitates were observed in the SMAT layer. The formation of nanograins in the surface layer after aging is attributed to recrystallization with controlled grain growth. The differential microstructures due to the chosen processing route have resulted in increased hardness of the surface layer and increased wear life of the material.

## INTRODUCTION

Inconel 718 is a high-strength Ni-based superalloy designed for moderate- to high-temperature (up to 650°C) applications.[1] It is a precipitation-strengthened material, where the primary strengthening phases at elevated temperatures are the $DO_{22}$ ordered $\gamma''$ phase and the $L_{12}$ ordered $\gamma'$ phase.[2,3] The material exhibits structural stability over a wide range of temperature. IN718 exhibits high yield strength, good ductility, high creep resistance, good fatigue strength and excellent weldability,[1,4] which makes it a suitable choice of material for gas turbines and other aerospace applications.[1,4,5] The alloy is predominantly used in compressors and turbines as discs and blades in land- and air-based gas turbine engines. Inconel 718 accounts for almost 50% of the total tonnage of superalloys used globally.[6]

Structural components subjected to dynamic loading, wear, fretting and fatigue are highly sensitive to the structure and properties of the surface. One of the novel ways to enhance surface-dependent properties is by nano-structuring the surface layer without changing its chemical composition,[7] which can be accomplished by generating a nano-structured surface layer through surface mechanical attrition treatment (SMAT).[8,9] In this process, hardened steel or ceramic balls bounce off a vibrating plate and strike the surface of the sample in random directions.

(Published online September 17, 2018)

A wide range of microstructures, ranging from nanocrystalline (near the surface, depths vary from ~ 20 $\mu$m to ~ 100 $\mu$m) to sub-micron and microcrystalline with increasing distance from the surface, have been reported in different materials subjected to SMAT.[8,9] The mechanism responsible for surface nano-crystallization during SMAT is severe plastic deformation with high dislocation activity and/or deformation twinning.[7]

The studies on IN718 have indicated that the nano-structured surface enhances its tensile, fatigue and fretting wear properties.[10–12] However, a high depth of influence (DOI) on surface treatment is desirable. The usual processing route employed for IN718 is a solution treatment followed by two-step aging (720°C/650°C) to obtain $\gamma''/\gamma'$ precipitates. Surface modification of IN718 in the aged condition has been performed by shot peening,[10] friction stir processing[13] and SMAT,[11,12] when the material is at its hardest and strongest form. This limits the increase in the surface hardness and the depth of the hardened surface layer (DOI) achieved. IN718 is relatively soft in solution treated condition. Thus, it would be better to perform surface treatment of material in the solutionized condition followed by precipitation aging. However, the strain induced during the former step in the surface layer may influence the precipitation behavior of the material. The aim of the present study is to study and contrast the precipitation in the surface-treated layer and the bulk of solution-treated IN718. The material has been subjected to surface modification via the SMAT process after the solution treatment stage, when the material is in its softest condition. The obtained material has been subjected to two-step aging treatment to promote the precipitation of the strengthening phases $\gamma''/\gamma'$ in the alloy.

## EXPERIMENTAL

### Material and Processes

Inconel 718 was received in overaged condition in the form of a bar. The nominal composition of the bar is given in Table I. Samples of dimension 25 mm × 25 mm × 1.4 mm were extracted from the bar and were subjected to solution treatment at 1095°C for 2 h followed by water quenching in order to dissolve all the precipitates into the matrix (henceforth, the solution-treated condition will be referred to as STQ). The STQ samples were metallographically polished before subjecting them to SMAT, which was performed using hardened steel balls (60 HRC) of 4.75 mm diameter at a vibrating frequency of 25 Hz and oscillation amplitude of 7.4 mm.

The SMAT process was carried out for two time durations, namely, 30 min and 60 min, in order to optimize the SMAT process. The 60 min of SMAT was characterized by higher surface hardness compared to the 30-min treated sample, hence the former was chosen for further processing (hereafter referred to as "STQ + SMAT"). The SMAT process and the corresponding sample nomenclature is pictorially depicted in Fig. 1a. To obtain a clear overview of the process, the temperature–time curve of the complete processing route adopted in the present study is shown in Fig. 1b.

The post-SMAT sample was then subjected to two-step aging in a vacuum with a heat treatment cycle consisting of the first heat treatment at 720°C for 8 h, followed by furnace-cooling at 55°C/h to 620°C, and the second heat treatment at 620°C for 8 h plus air-cooling (hereafter referred to as STQ + SMAT + AGED).

### Microstructural Characterization

For microstructural characterization, the samples were sectioned along the transverse section. This section was subjected to metallographic polishing followed by etching in acetic glycergia (15 mL HCl + 10 mL $HNO_3$ + 10 mL acetic acid + 1 drop glycerol) and examined under an optical microscope (Carl Zeiss Axio Observer 5) as well as a scanning electron microscope (FEI Sirion FE-SEM). The cross-section of the STQ + SMAT + AGED sample was electropolished before examination under SEM. Finer microstructural details of the SMAT region before (STQ + SMAT) and after (STQ + SMAT + AGED) aging, and, the undeformed bulk region (STQ + AGED) were investigated using transmission electron microscopy (TEM; TECNAI G2 F30). In order to prepare samples for TEM, discs with 3 mm diameter were extracted from the appropriate region. The discs were mechanically polished to 100 $\mu$m followed by dimple grinding to create a crater in the middle of the disc. For the STQ + SMAT and STQ + SMAT + AGED samples, dimpling was carried out on the surface opposite to the SMAT surface. The samples were then subjected to precision ion milling (Gatan PIPS) to obtain an electron transparent region for TEM examination. For the STQ + AGED sample (without SMAT), discs of 3 mm diameter were obtained by dimple grinding followed by electropolishing in a solution consisting of 10% perchloric acid and 90% methanol, cooled to − 30°C using a twin jet electropolisher (FISHIONE, Model 110) operated at 12 V and 20 mA. The as-

**Table I. Chemical composition of Inconel 718 used in the present study**

| Element | Ni | Fe | Cr | Nb | Mo | Ti | Al | Mn | Si | C | Cu | S | P |
|---|---|---|---|---|---|---|---|---|---|---|---|---|---|
| wt.% | Balance | 19.53 | 18.4 | 5.17 | 3.10 | 1.04 | 0.49 | 0.01 | 0.2 | 0.02 | 0.014 | 0.002 | 0.005 |

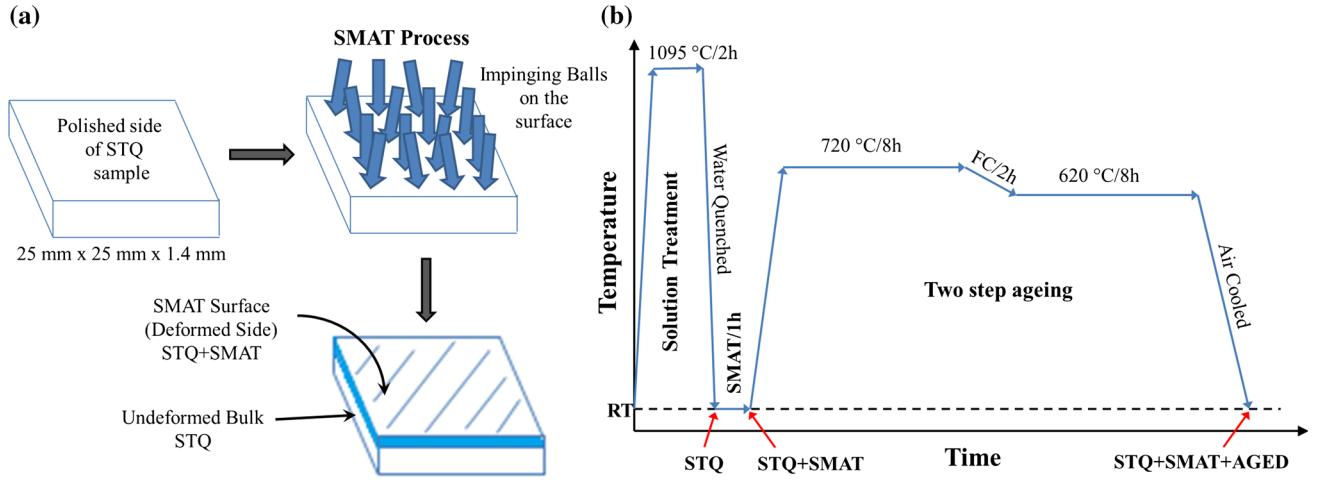


Fig. 1. (a) Schematic of the SMAT process with corresponding sample nomenclature. (b) Temperature–time curve of the complete processing route adopted.

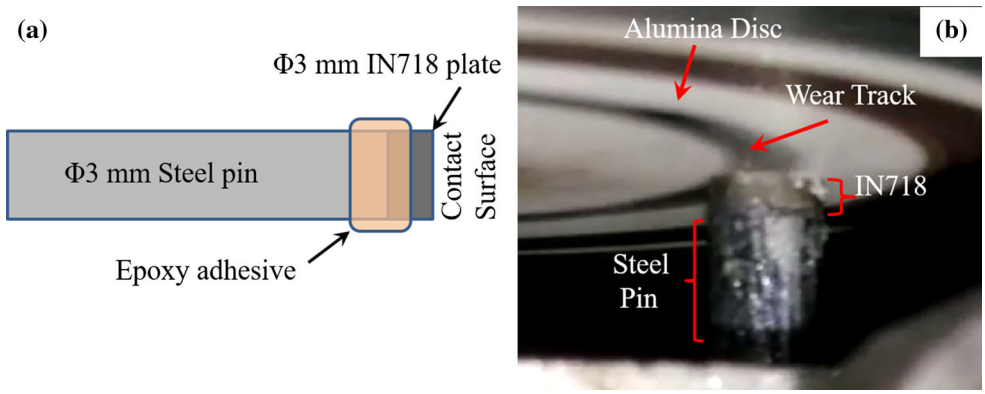


Fig. 2. (a) Schematic of the modified pin. (b) Wear test being carried out on the modified pin.

prepared foils were examined under TEM operating at 300 kV.

## Mechanical Testing

The relevant mechanical properties of the samples were determined by hardness and wear tests. In order to determine the hardness, Vickers microhardness was measured using a microhardness testing machine (Future-Tech FV-810) at a load of 25 g with 10-s dwell time for the samples obtained after different stages of processing. A rather low load was selected for hardness measurement, in order to limit the indented volume within the SMAT-affected zone. To examine the wear properties of the materials, a 'pin on disc' wear test was carried out on the SMAT surface as well as on the undeformed surface of the aged samples (Fig. 2b). Modified pins of 3 mm diameter were fabricated to carry out the pin-on-disc wear tests by securing the sample disc on a steel pin. The experimental scheme is shown in Fig. 2a. For the wear test, an alumina disc (hardness 1600 ± 144 HV) was used as the contact surface. The test was carried out under a load of 7 N for a sliding distance of 54 m with 0.1 m/s linear velocity between the pin and the disc at room temperature in air. The low load (7 N) was selected for the test so that less than 20 $\mu$m thickness of material is removed from the surface and the wear property of only the SMAT-affected zone could be estimated (SMAT-deformed layer thickness was about 30–40 $\mu$m).

# RESULTS

## Microstructural Characterization of the Materials

The SEM micrograph of the as-received IN718 (Fig. 3a) shows precipitates present in the microstructure. The $\delta$ precipitate revealed in Fig. 3a are observed primarily at the grain boundaries. The as-received IN718 was subjected to solution treatment. The optical micrograph of the STQ sample reveals the presence of equiaxed grains (Fig. 3b). The $\delta$ and primary $\gamma''$ precipitates along with the carbide (MC) phase were not observed in the microstructure of the starting STQ sample.

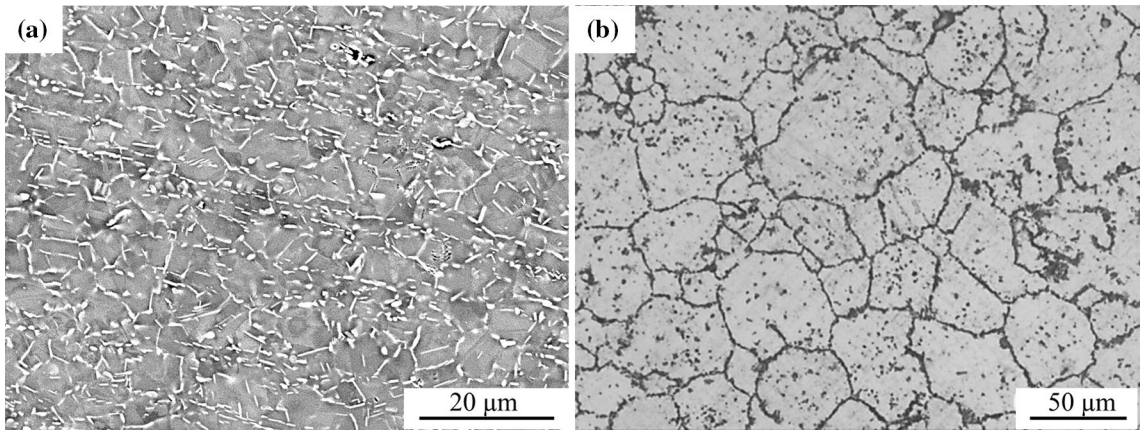


Fig. 3. (a) SEM micrograph of the as-received IN718 displaying $\delta$ precipitates. (b) Optical micrograph of the STQ sample displaying a single phase equiaxed microstructural feature.

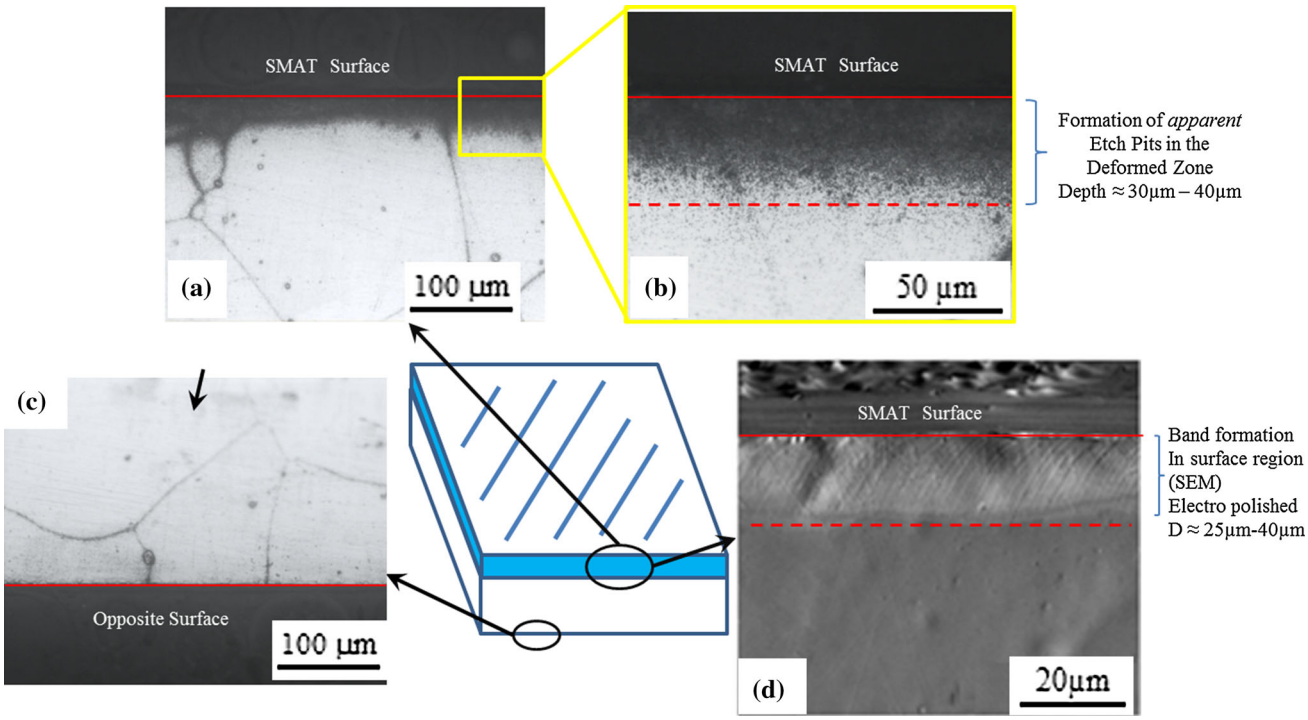


Fig. 4. Cross-sectional micrographs of STQ + AGED and STQ + SMAT + AGED samples. Both the representative regions are present in the same sample. (a, b) Optical micrographs near the SMAT surface, (c) optical micrograph in the undeformed region (the side opposite to the SMAT surface), and (d) SEM micrograph of the electropolished sample.

Therefore, an equiaxed, precipitate-free microstructure was used as the starting microstructure for further processing.

The cross-sections of the STQ + AGED and STQ + SMAT + AGED samples were also examined under the optical microscope. The two representative samples correspond to different regions in the same sample (undeformed bulk and SMAT surface). Intensive etch pits were revealed below the SMAT surface (STQ + SMAT + AGED) to a depth of about 30–40 $\mu$m (Fig. 4a and b). To ascertain that the etch pits are not a byproduct of metallurgical polishing near the surface, an optical micrograph for the STQ + AGED sample was taken near the surface on the opposite side of the sample (depicted in Fig. 4). No etch pits were observed in the STQ + AGED sample (Fig. 4c). This confirms that the pits were not due to polishing issues at the surface (edge), but were present due to the effect of SMAT. The high defect density at the SMAT surface led to pitting of the surface on etching. To avoid the pits, the cross-section of STQ + SMAT + AGED was electropolished and examined. The SEM image of the STQ + SMAT + AGED sample (Fig. 4d) near the surface revealed the presence of bands near the SMAT surface to a depth of about 25–40 $\mu$m. It was

observed that the DOI (band thickness from surface) was heterogeneous and varied within a grain as well as between grains. It should be noted that the $\delta$ precipitate and primary $\gamma''$ precipitate were not observed in either of the samples.

## Transmission Electron Microscope Investigations

Optical and SEM micrographs were not able to provide and resolve the finer features in the microstructure, which are expected in the material subjected to the SMAT process. Hence, the materials were further examined under TEM to study finer microstructural features. STQ + SMAT, STQ + AGED and STQ + SMAT + AGED samples were investigated to obtain a complete understanding of the microstructural evolution undergone at various steps during the adopted processing route and are discussed in the subsequent subsections.

### *STQ + SMAT*

The bright field TEM micrographs for the STQ + SMAT sample are shown in Fig. 5a, b, c and d. Figure 5a reveals the presence of bands in the SMAT layer which primarily consists of dislocations. A few long elongated nanotwins are also observed in the microstructure, indicated by arrows in Fig. 5b. However, such twins are observed sparsely spaced and twin bundles are not observed. A closer look into the band reveals a region subdivided into nanodomains (Fig. 5c and d). Nanotwin-type features are present in some regions in bands, as indicated by arrow in Fig. 5c. Moreover, the bands mainly consist of strained regions due to heavy dislocation activity. The [112] zone axis diffraction pattern of the region in Fig. 5d is shown as an inset. The diffraction pattern consists of distinct individual diffraction spots along with very weak twin spots. The ring-type pattern usually observed in nano-crystalline material is not observed. This indicates that, although nanodomains are present in the microstructure, the misorientation across such region is limited and the domains formed have similar orientation. It can be said that complete nano-crystallization with random orientation was not achieved after SMAT. The weak intensity of twin spots indicates the low volume fraction of nanotwins. No evidence of any precipitates were observed which shows the absence of stress-induced precipitate formation upon SMAT.

### *STQ + AGED*

The bright field TEM micrograph and diffraction pattern with the zone axis [110] for STQ + AGED sample are shown in Fig. 6a and b, respectively. Figure 6a reveals the presence of plate-like secondary $\gamma''$ precipitates which are identified from their shape and small size (a few nm). The spots for the same are observed in the [110] zone axis diffraction pattern of the same region, as indicated by the arrow in Fig. 6b, which is in line with earlier reports.[13,14] The distinct diffraction spots corresponding to the $\gamma$ matrix indicate the microcrystalline grain size.

### *STQ + SMAT + AGED*

Figure 7a displays the bright field micrograph of the STQ + SMAT + AGED sample and reveals the nano-crystalline characteristics of the sample (indicated by the arrow). The corresponding diffraction pattern (inset in Fig. 7a) shows a ring pattern, which is typical of a nano-crystalline material. The dark field micrographs at different magnification are shown in Fig. 7b, c and d. The dark field micrograph (Fig. 7b) clearly provides the evidence of nano-crystalline grains. Moreover, it can be seen in Fig. 7c that the microstructure of the STQ + SMAT + AGED sample consists of nanodomains of size 30–50 nm which are further divided by parallel banded features of nanometer size (width $\sim$ 5 nm), as indicated by the arrow in the micrograph. This gives an indication of nanotwins in the microstructure. The parallel nanometer-sized band-like features are clearly discernible in Fig. 7d. Apart from the nanotwins, equiaxed regions are also observed in the microstructure of the STQ + SMAT + AGED sample.

## Mechanical Properties of the As-Processed Samples

Microhardness measurements were carried out to study the effect of processing route on the mechanical properties. The hardness of the STQ sample was obtained to be $295 \pm 6$ HV, while that of the STQ + SMAT sample was $350 \pm 5$ HV. Thus, the hardness of the solution-treated sample increased by $\sim$ 19% as a result of the surface modification of via SMAT. After aging, the hardness of the STQ + AGED sample (bulk) increased to $375 \pm 30$ HV and that of the STQ + SMAT + AGED sample increased to $530 \pm 20$ HV. Thus, SMAT has been found to be beneficial in improving the overall mechanical property, resulting in a $\sim$ 41% increase in hardness. The increased surface hardness of the STQ + SMAT + AGED sample is expected to significantly improve the wear properties.

The wear test was primarily carried out to quantify the improvement in wear resistance of the material after aging. The results of the wear test for the STQ + AGED and STQ + SMAT + AGED samples are listed in Table II. An enhancement of wear resistance by $\sim$ 131% is observed for the STQ + SMAT + AGED-processed sample when compared to the STQ + AGED sample. The enhancement in wear resistance is attributed to the presence of nanostructures on the surface of the STQ + SMAT + AGED sample.

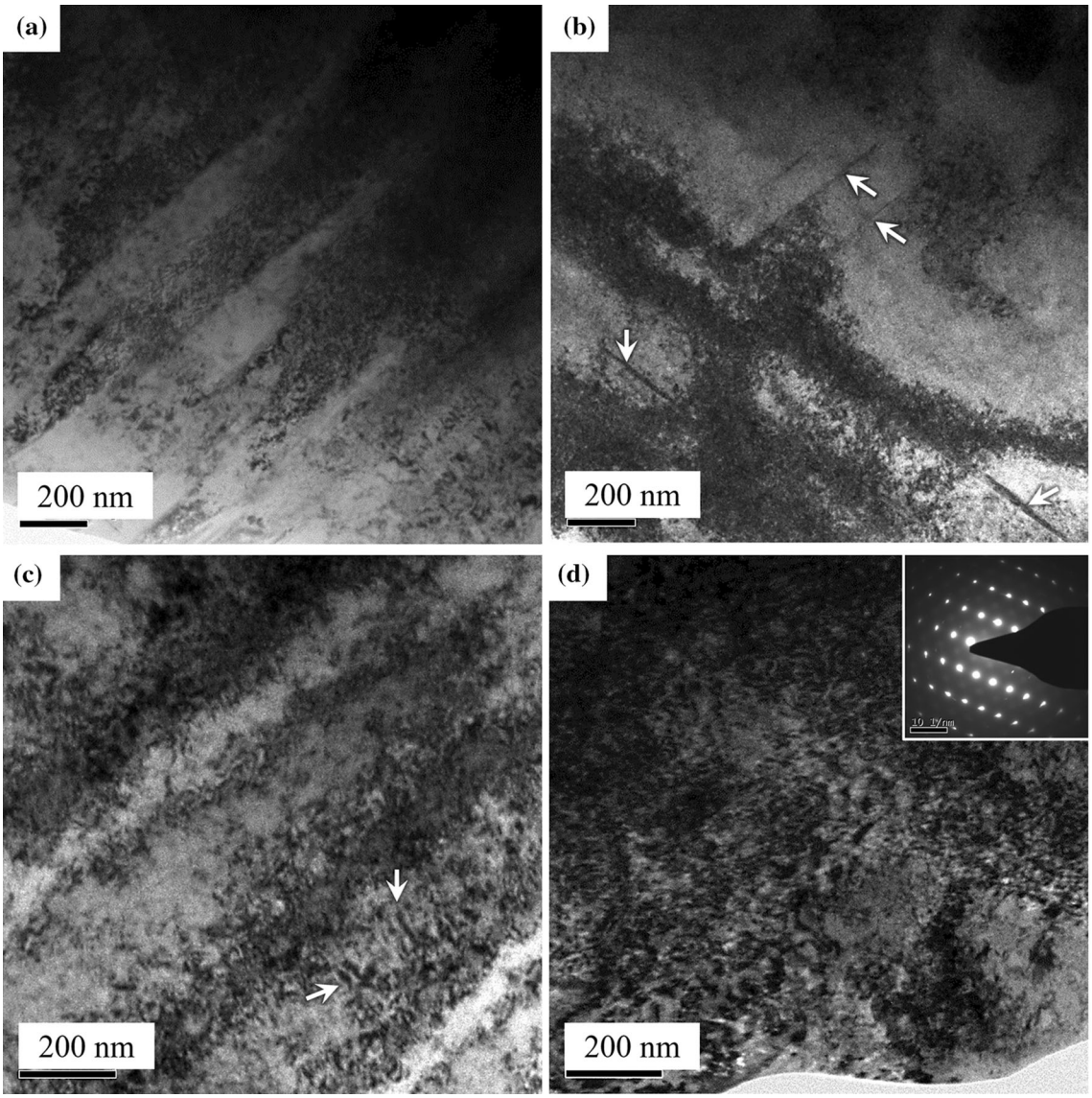


Fig. 5. (a–d) Bright field TEM micrographs for the STQ + SMAT sample. The diffraction pattern along the [112] zone axis for (d) is shown in the inset.

## DISCUSSION

The processing route employed in the present study (solution treatment + SMAT + aging) yielded a better surface hardness and wear resistance in the material. Improvement in both the mechanical properties could be attributed to the presence of surface nanostructures with nanotwins as a result of the severe plastic deformation imparted by SMAT on the surface layer. A subsequent two-step heat treatment (720°C/8 h + 620°C/8 h) further led to the enhancement in the properties. The findings of the present study in terms of the mechanisms leading to the evolution of microstructures during various steps of processing is further discussed.

### Microstructural Evolution During SMAT

Bands along with nanodomains and nanotwins are observed after SMAT in the STQ + SMAT sample. Nano-crystallization of the surface via SMAT is reported to occur through many ways. In Fe,[15] the transformation takes place via the development of dense dislocation walls and dislocation tangles into sub-boundaries which eventually transform into high-angle boundaries. In Cu,[16] nanocrystallization occurs via transformation of dislocation cells into high-angle boundaries at the subsurface, while in AISI 304 stainless steel (low SFE), it is reported to take place via the formation and intersection of planar dislocation arrays with twins and

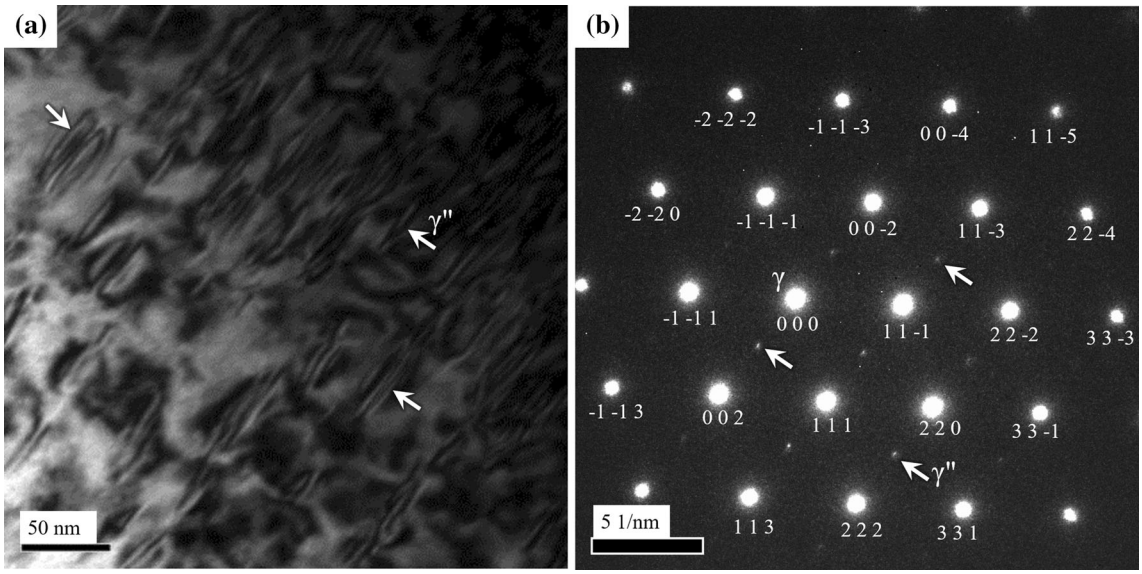


Fig. 6. (a) Bright field TEM micrograph and (b) diffraction pattern along the zone axis [110] for the STQ + AGED sample.

twin–twin interactions.[17] Moreover, the governing mechanism also varies with the depth from the SMAT surface.[16] IN718 has a stacking fault energy (SFE)[18] of 50 mJ/m$^2$. Tao et al.[19] reported that grain subdivision in IN600 (SFE[20] $\sim$ 28 mJ/m$^2$) occurs via interaction of mechanical microtwins with dislocations. The SFE of IN718 is higher than this value, but it can still be categorized as a low SFE material. The presence of dislocation bands along with a few elongated nanotwins and the few nanotwin-type features within the bands in the microstructure of the STQ + SMAT sample (Fig. 5) indicates multiple mechanisms, comprising dislocation activity and twin activity, to be active, which results in the formation of nanodomains. This proceeds via the interaction of dislocation arrays with twins and twin–twin interactions. The present microstructural findings are in partial agreement with an earlier study on the surface modification of IN718,[19] where the formation of nanometer-sized grains was reported, which did not contain nanotwins. Moreover, it should be noted that, in the present study, the diffraction pattern of the region within bands shows individual spots. Thus, it can be said that the nanodomains formed do not have random orientations in the true sense and that the process of nanocrystallization is not complete in the heavily strained SMAT layer.

## Microstructural Evolution in SMAT Layer on Aging

The microstructure of the STQ + SMAT + AGED sample (Fig. 7) has distinct nanograins ($\sim$ 30–50 nm) with nanotwins ($\sim$ 5 nm width) and no evidence of any precipitates. The microstructure after aging (Fig. 7) has considerably transformed after aging treatment from that of SMAT (Fig. 5), which is evident from their corresponding microstructures and diffraction patterns. The evolution of microstructure from SMAT upon aging is attributed to the onset of recovery and recrystallization during the aging treatment. The strained bands along with nanotwins present in the SMAT microstructure act as potential sites for recrystallization nuclei formation and, thus, aids in the recrystallization process. Nevertheless, the grain size after aging is still in the nanometer scale. This indicates that grain growth was minimal during the aging process. This was expected as the temperature range adopted during the aging (720°C/8 h + 620°C/8 h) is around $T/T_m \sim 0.5$–$0.6$. The temperature is high enough to promote the formation of recrystallized nuclei in the heavily strained SMAT layer. However, the grain growth of the nuclei is limited in this temperature range. This is due to the fact that the grain boundary mobility is lower at lower $T/T_m$ and increases with an increase in $T/T_m$. The local recrystallization process results in the formation of nanograins with high-angle grain boundaries. This transformation in the microstructure upon aging results in an increase in hardness from 350 HV (for STQ + SMAT) to 530 HV (for STQ + SMAT + AGED) in $T/T_m$ SMAT layer.

## Difference in the Precipitation Behavior of STQ and STQ + SMAT Region on Aging

No evidence of precipitation was observed in the STQ + SMAT + AGED sample after aging. In contrast, the STQ + AGED sample consists of a microcrystalline $\gamma$ matrix containing $\gamma''$ precipitates. The difference in the precipitation behavior of the STQ + AGED and STQ + SMAT + AGED samples during the two-step aging can be comprehended by understanding the precipitation behavior of IN718 in general. The needle-like and globular $\delta$

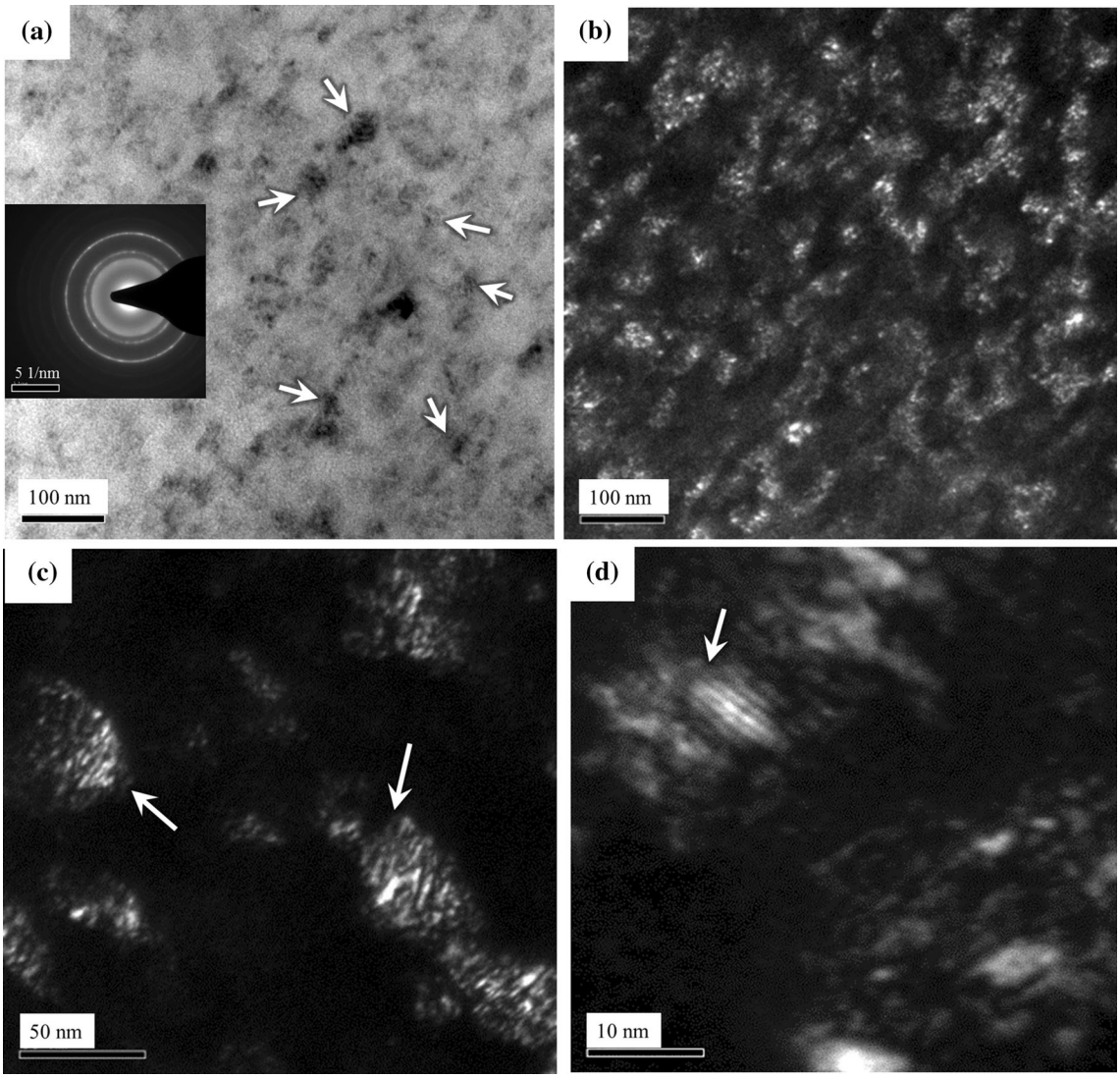


Fig. 7. TEM micrographs of the STQ + SMAT + AGED sample. (a) bright field and, (b–d) dark field TEM micrographs at different magnifications. Inset in (a) shows the corresponding diffraction pattern.

**Table II. Results of wear test**

| Wear parameters | STQ + AGED | STQ + SMAT + AGED |
|---|---|---|
| Change in mass after tests ($\Delta m$) | 0.0010 g | 0.0004 g |
| Volumetric loss ($\Delta V$) | $1.216 \times 10^{-1}$ mm$^3$ | $4.866 \times 10^{-2}$ mm$^3$ |
| Wear rate ($W$) | $2.085 \times 10^{-3}$ mm$^3$/m | $9.011 \times 10^{-4}$ mm$^3$/m |
| Specific wear rate ($W_{sp}$) | $2.979 \times 10^{-4}$ mm$^3$/Nm | $1.287 \times 10^{-4}$ mm$^3$/Nm |
| Wear resistance ($W_r$) | 479.61 m/mm$^3$ | 1109.75 m/mm$^3$ |

precipitates ($\sim 1\ \mu$m) are observed primarily at grain boundaries, when the solutionized IN718 is heat-treated at 870°C.[21] The formation of plate-like coarse lenticular primary $\gamma''$ precipitates ($\sim 0.3\ \mu$m) has been reported in the the matrix and at grain boundaries, on aging at 870 °C. In contrast, secondary $\gamma''$ precipitates form at 760°C and are lenticular in shape (10–40 nm),[21] whereas the $\gamma'$ precipitates are favored at 760°C and 650°C. These precipitates are globular/cuboidal in shape (10–40 nm).[21] The morphology of the $\gamma'$ precipitate is attributed to the cube-to-cube orientation relationship with the $\gamma$ matrix.[22] It should be noted that $\gamma'$ precipitates, as small as 5–6 nm, have also been observed.[23] Moreover, at 680°C, $\gamma'$ precipitation precedes secondary $\gamma''$ precipitation.[23] At 860°C,

cold working promotes the precipitation of the $\delta$ phase and has an inverse effect on $\gamma''$.[24] On two-step aging of cold-worked (up to 50%) IN718,[25] the precipitation kinetics (growth) of $\gamma''$ is reduced and it loses coherence with the matrix, resulting in modification of the shape of the precipitate. In contrast, Cai et al.[26] reported an accelerated $\gamma''$ precipitation kinetics in the initial stages of the two-step aging process in the shot-peened IN718. Song et al.[13] reported accelerated formation of the $\gamma'$ precipitate on two-step aging after friction stir processing. In the present study, the $\delta$ precipitate were not observed in either the STQ + AGED or the STQ + SMAT + AGED samples, as the two-step aging process adopted did not favor its precipitation. In the bulk STQ + AGED sample, which was aged from the solution-treated condition, secondary $\gamma''$ precipitates were observed, as seen from the TEM micrograph and diffraction pattern (Fig. 6). In contrast, precipitates were not observed in the TEM micrographs of the STQ + SMAT + AGED sample (Fig. 7). The microstructure of the STQ + SMAT + AGED sample shows nanograins with nanotwins ($\sim$ 5 nm). The limiting size of the grains is expected to inhibit the precipitation of large plate-like primary $\gamma''$ precipitates. Moreover, the changing orientation of the grains of the $\gamma$ matrix (nanograins with nanotwins) over small distancse ($\sim$ 5 nm) is likely to hinder the growth of the precipitates as a result of the loss of coherency of the precipitate. As coherency with the $\gamma$ matrix is one of the prime reasons for the stabilization of the metastable $\gamma''$ precipitate, the circumstances in the nanograins are not favorable for $\gamma''$ precipitation. However, as reported earlier,[23] there is a possibility for the formation of $\gamma'$ precipitates with globular shape which are smaller in size (a few nm). Some globular regions of nanoscale were observed in the STQ + SMAT + AGED sample (Fig. 7d). Nevertheless, the presence of $\gamma'$ precipitates in the STQ + SMAT + AGED sample could not be confirmed in the present study, as deduced from the diffraction pattern. Further EDS investigation of the microstructure of the STQ + SMAT + AGED sample could help in resolving the issue and will be carried out in future.

## CONCLUSION

The processing route often chosen in previous studies in the literature follow the sequence solution treatment—aging—surface deformation technique—annealing. In the present study, the processing route has been modified to reduce the number of steps and to increase the positive impact of surface modification on material properties. The material is subjected to surface mechanical attrition treatment (SMAT) after solution treatment, followed by a two-step aging treatment which promotes precipitation of $\gamma''/\gamma'$ in the alloy. The microstructure of the bulk aged material consists of microcrystalline grains with $\gamma''$ precipitates, while that of the surface layer consists of nanograins with nanotwins. However, the $\gamma''/\gamma'$ precipitates were not observed in the surface-treated layer. The processing route chosen has resulted in an increased surface hardness and wear resistance of the material, which is attributed to the surface nanostructure with nanotwins. The absence of precipitation in the surface layer is attributed to the limiting size of the surface nanograins (size $\sim$ 5 nm) which are likely to hinder the growth of precipitates.

## ACKNOWLEDGEMENTS

Funding from the Department of Science and Technology (India) through Grant DST/RC-UK/14-AM/2012 and Engineering and Physical Sciences Research Council (UK) through grant EP/K028316/1 for the project “Modeling of Advanced Materials for Simulation of Transformative Manufacturing Processes (MAST)” is gratefully acknowledged. We also thank Dr. Rajib Kalsar for helping with TEM imaging of STQ + SMAT sample.

## REFERENCES

1. R.E. Schafrik, D.D. Ward, and J.R. Groh, *Application of Alloy 718 in GE Aircraft Engines: Past, Present and Next Five Years* (Warrendale: TMS, 2001), p. 1.
2. Y. Huang and T.G. Langdon, *Mater. Sci. Eng., A* 410–411, 130 (2005).
3. M.C. Chaturvedi and Y.-F. Han, *Metal Sci.* 17, 145 (1983).
4. T.S. Byun and K. Farrell, *J. Nucl. Mater.* 318, 292 (2003).
5. J. F. Barker, in *The Initial Years of Alloy 718: A GE Perspective*, 1989 (TMS), p. 269.
6. S.G. Tian, J.H. Zhang, H.H. Zhou, H.C. Yang, Y.B. Xu, and Z.Q. Hu, *Mater. Sci. Technol.* 14, 751 (1998).
7. N.R. Tao, J. Lu, and K. Lu, *Mater. Sci. Forum* 579, 91 (2008).
8. K. Lu and J. Lu, *Mater. Sci. Eng. A* 375–377, 38 (2004).
9. J. Azadmanjiri, C.C. Berndt, A. Kapoor, and C. Wen, *Crit. Rev. Solid State Mater. Sci.* 40, 164 (2015).
10. S. Kumar, G. Sudhakar Rao, K. Chattopadhyay, G.S. Mahobia, N.C. Santhi Srinivas, and V. Singh, *Mater. Des. (1980–2015)* 62, 76 (2014).
11. S. Anand Kumar, S. Ganesh Sundara Raman, and T.S.N. Sankara Narayanan, *Trans. Indian Inst. Met.* 65, 473 (2012).
12. S. Anand Kumar, S. Ganesh Sundara Raman, T.S.N. Sankara Narayanan, and R. Gnanamoorthy, *Surf. Coat. Technol.* 206, 4425 (2012).
13. K.H. Song, W.Y. Kim, and K. Nakata, *Mater. Trans.* 54, 2032 (2013).
14. H.R. Zhang and O.A. Ojo, *J. Mater. Sci.* 43, 6024 (2008).
15. N.R. Tao, Z.B. Wang, W.P. Tong, M.L. Sui, J. Lu, and K. Lu, *Acta Mater.* 50, 4603 (2002).
16. K. Wang, N.R. Tao, G. Liu, J. Lu, and K. Lu, *Acta Mater.* 54, 5281 (2006).
17. H.W. Zhang, Z.K. Hei, G. Liu, J. Lu, and K. Lu, *Acta Mater.* 51, 1871 (2003).
18. D. Fournier and A. Pineau, *Metall. Trans. A* 8, 1095 (1977).
19. N. Tao, H. Zhang, J. Lu, and K. Lu, *Mater. Trans.* 44, 1919 (2003).
20. L.E. Murr, *Thin Solid Films* 4, 389 (1969).
21. M.G. Burke and M.K. Miller, *Precipitation in Alloy 718: A combined AEM and APFIM Investigation* (Warrendale: TMS, 1991), p. 337.

22. M. Sundararaman, P. Mukhopadhyay, and S. Banerjee, *Metall. Trans. A* 23, 2015 (1992).
23. C. Slama and M. Abdellaoui, *J. Alloys Compd.* 306, 277 (2000).
24. W.C. Liu, F.R. Xiao, M. Yao, H. Yuan, Z.L. Chen, Z.Q. Jiang, S.G. Wang, and W.H. Li, *J. Mater. Sci. Lett.* 17, 245 (1998).
25. M.P. Solignac, M. Foucault, and J.M. Cloue, in *Effects of Cold Working on Microstructural and Mechanical Properties and SCC Behavior of Alloy 718*, 1994 (TMS), p. 751.
26. D. Cai, P. Nie, J. Shan, W. Liu, Y. Gao, and M. Yao, *J. Mater. Eng. Perform.* 15, 614 (2006).